The Role of Gravity Waves in Slowly Varying in Time Mesoscale Motions

G. L. BROWNING

Cooperative Institute for Research in the Atmosphere, Colorado State University, Fort Collins, Colorado

H.-O. KREISS

Department of Mathematics, University of California, Los Angeles, Los Angeles, California

(Manuscript received 16 April 1996, in final form 11 October 1996)

ABSTRACT

Pressure oscillations with amplitudes of the deviations from the horizontal mean and periods considerably less than those for the large-scale case have been observed in a number of summer and winter storms. However, there is conflicting evidence about the role of these waves in mesoscale storms. In the case of mesoscale heating that is a prescribed function of the independent variables, it has been proven that the dominant component of the corresponding slowly varying in time solution is accurately described by a simple dynamical (reduced) system in which gravity waves play no role. This paper proves that large spatial-scale gravity waves with amplitudes and periods of the pressure perturbations the same as the reduced system component of the solution can be generated by mesoscale storms. Because the amplitudes and the periods of the pressure perturbations for the two components of the solution are similar, it is difficult to distinguish between them using temporal plots of the pressure at a single location, and this is the source of a large part of the confusion about these waves. This problem, in conjunction with the fact that the vertical velocity of the gravity waves is an order of magnitude smaller than the maximum vertical velocity in the dominant component of the solution (and therefore in the noise range of current wind profilers), makes observation of gravity waves very difficult. In numerical simulations, if both components of the mesoscale solution are required, the lateral extent of the domain of solution must be considerably larger than the lateral extent of the mesoscale heating in order that the large-scale gravity waves be correct. In this case, it is shown that the multiscale system for meteorology developed earlier by Browning and Kreiss accurately describes both components of the solution.

1. Introduction

Pressure oscillations with amplitudes of the deviations from the horizontal mean and periods considerably less than those for the large-scale case have been observed in a number of summer and winter storms (Brunk 1949; Pothecary 1954; Clarke 1962; Wagner 1962; Eom 1975; Stobie et al. 1983; Bosart and Sanders 1986; Uccellini and Koch 1987; Ralph et al. 1993). However, there is conflicting evidence about the role of these waves in mesoscale storms. Some observations seem to indicate a substantial degree of interaction of these waves with a storm, while others indicate just the opposite. For example, Bosart and Sanders (1986) make the following statements in section 4b of their paper: ''Thus it seems that the undeniable effect of the wave on overhead condensation rate is not clearly related to ground accumulation, owing to complexity of physical process and to difficulty of observations. . . . The wave propagates entirely through the high cloud shield, however, and its effect is not dramatic.'' In this study an explanation for these contradictory observations is provided. Also, the longevity of the gravity waves in many of these studies is ascribed to ducting (Lindzen and Tung 1976). Here a different mechanism, the longwave portion of the heating, is shown to be capable of producing long-lived, large-scale gravity waves.

There are two important questions related to possible interactions of gravity waves with other motions in the atmosphere. The first question is whether or not these waves can initiate new storms in areas of unstable air located some distance from their origin. If this is true, then it is unlikely that current numerical forecast models can predict this triggering mechanism for the following reasons. In the first place, the waves are not observed accurately because of their short timescales. Thus the observational data are unlikely to contain the correct information about these waves. Even if the waves were properly represented in the observed data, most global

*Current affiliation: NOAA/ERL Forecast Systems Laboratory R/E/FS, Boulder, Colorado.

Corresponding author address: Dr. Gerald L. Browning, NOAA/ERL/R/E/FS, Forecast Systems Laboratory, 325 Broadway, Boulder, CO 80303.
E-mail: browning@fsl.noaa.gov

© 1997 American Meteorological Society

models remove them from the solution by various initialization methods before using the data in the model. Other models assimilate observational data without initialization, which can create spurious gravity waves (Daley 1991; Browning and Kreiss 1995). If gravity waves can initiate storms, it is conceivable that these artificially generated gravity waves could create artificial storms. On the other hand, limited-area models do not allow gravity waves to propagate into or out of an open boundary in the same manner as if the boundary was not present. Thus it cannot be expected that a limited-area model will correctly capture the creation of a new storm by a gravity wave, unless the wave is accurately described by the observed data and is completely unaffected by the boundaries during the period of integration (this is difficult to ensure when the waves propagate fairly fast). The alternative assumption, that is, that these waves do not create new storms, is certainly more appealing, but possibly unrealistic.

The second question is whether or not these waves interact with a mesoscale storm in progress. In this paper, two possibilities related to this question will be analyzed. The possibilities are distinguished by the relationship of the horizontal length scale of the mesoscale heating to the lateral size of the domain of solution, that is, if the length scale of the heating is the same as or smaller than the lateral size of the domain of solution. In both cases it will be shown that the gravity waves that are generated are a small part of the complete solution and their interaction with the dominant component of the solution is very small. Although this result at first seems to contradict some of the observations, the apparent paradox can be resolved by considering the nature of slowly varying in time mesoscale motions; in particular, in the absence of topography, mesoscale motions with vertical velocities $O(1)$ m s^{-1} can exist only in the presence of heating (Browning and Kreiss 1986). As a particular example, many of the pressure oscillations appear as a single wave (e.g., Sanders and Bosart 1985) and are described as being gravity waves similar to the schematic diagram developed by Eom (1975). However, these arguments are not sufficient to preclude the possibility that the oscillations correspond to a cooling–heating couplet moving through or with the storm (F. M. Ralph 1995, personal communication). In fact, Bosart and Sanders (1986) make the following statements: ''Whether the accompanying convection and enhancement of condensation heating represented a forcing effect on the wave is unknown because of uncertainties concerning its vertical structure, but circumstantial evidence indicates that the answer is probably yes.'' This statement allows for the possibility that the oscillations might well be forced by local heating–cooling effects, which agrees with the mathematical results to follow.

The first step in understanding mesoscale motions is to scale the equations of motion using typical scaling parameters for those motions. In section 2, two scalings representing typical sizes for the vertical velocity in mesoscale storms are introduced. Section 3 considers the case when the lateral extent of the mesoscale heating is approximately the same as the lateral size of the domain of solution. In this case it is proved that the multiscale system introduced earlier by Browning and Kreiss (1986) can describe the dominant component of the corresponding slowly varying in time mesoscale solution up to a relative error term $O(10^{-2})$. In this case it is possible to show that the small-amplitude gravity waves that are generated essentially do not interact with the part of the solution that to first approximation is described by the reduced system (Kreiss et al. 1991). Although many mesoscale simulations use a lateral domain size somewhat larger than the lateral extent of the heating, in reality mesoscale storms are embedded in a domain whose lateral size is two orders of magnitude larger than the lateral extent of the heating. Section 4 provides an analysis of this case and provides insight into why gravity waves are generated in this case and why their interaction with the part of the mesoscale solution that is accurately described by the reduced system is minimal. Section 5 contains numerical examples to illustrate a number of the theoretical results. Conclusions are presented in section 6.

2. Mesoscale motions

The Eulerian equations that describe three-dimensional atmospheric motions have been scaled for flows that are slowly varying in time and space (Browning and Kreiss 1986). The scaling parameters $L_1(U)$, $L_2(V)$, and $D(W)$ are the representative length (velocity component) scales along the x, y, and z axes, respectively, and S_1 represents the maximum size of the deviation of the pressure on a given height from the horizontal mean of the pressure on that height divided by the mean. In a typical mesoscale storm, there are two distinct regions: convective towers in front of stratiform rain (Houze 1989). Because the scaling in either region leads to similar conclusions, only the stratiform rain region will be considered. For this region consider the parameters

$$L_1 = L_2 = 100 \text{ km}, \quad D = 10 \text{ km}, \tag{2.1a}$$

$$U = V = 10 \text{ m s}^{-1}, \; W = 1 \text{ m s}^{-1}, \quad S_1 = 10^{-3}, \tag{2.1b}$$

where the timescale T is given by $T = L_1/U$, which is on the order of a few hours. Houze (1989) states that the maximum vertical velocity is approximately 0.5 m^{-1} s^{-1}. While nonintegral values for the vertical velocity may be used, the value above leads to a simpler scaled system and the same conclusions. The corresponding dimensionless system that describes slowly varying motions is (Browning and Kreiss 1994a)

$$\frac{ds}{dt} - \varepsilon^{-2}\tilde{s}(w - H) = 0, \tag{2.2a}$$

$$\frac{du}{dt} + \rho_0^{-1}p_x - fv = 0, \tag{2.2b}$$

$$\frac{dv}{dt} + \rho_0^{-1}p_y + fu = 0, \tag{2.2c}$$

$$\frac{dw}{dt} + \epsilon^{-2}(\rho_0^{-1}p_z + \tilde{p}p + gs) = 0, \tag{2.2d}$$

$$\frac{dp}{dt} + \epsilon^{-3}wp_{0z} + \epsilon^{-3}\gamma p_0(u_x + v_y + w_z) = \epsilon^{-2}G, \tag{2.2e}$$

where s is proportional to the reciprocal of the potential temperature (the variable s is used for consistency with earlier work); $\mathbf{V} = (u, v, w)^T$ is the velocity (the superscript T denotes the transpose); p is the pressure; $d/dt = \partial/\partial t + u\partial/\partial x + v\partial/\partial y + w\partial/\partial z$, $\varepsilon = 10^{-1}$; f is the (dimensionless) Coriolis parameter; g is the (dimensionless) gravity; $\gamma = 1.4$; and $\tilde{s}(z)$, $\rho_0(z)$, $\tilde{p}(z)$, and $p_0(z)$ are $O(1)$ functions determined by the mean state of the atmosphere and are the same for all scales (Browning and Kreiss 1986). The $O(1)$ heating terms H and G are assumed to be slowly varying functions of the independent variables. Because the heating term G does not affect the arguments to follow, for simplicity of presentation it will be assumed to be zero.

A brief discussion of the assumption of prescribed heating is in order. Numerous authors (e.g., Gill 1980; Kasahara 1984) have explicitly prescribed heating terms as functions of the independent variables and analyzed the resulting flow so there is precedence for making such an assumption. However, this assumption is not as restrictive as it might first seem. A model with the correct functional form of the heating could be run and the heating at each time step of the integration saved on disk. Then the model could be run with the heating for each step being read in from the disk. In the latter case, the heating behaves exactly as if it were a prescribed function of the independent variables.

If the solution of system (2.2) did not have a component that was essentially independent of gravity waves, that is, if the gravity waves are as important as the advective waves and substantially interact with them as some authors have stated (e.g., Skamarock and Klemp 1994), then a numerical approximation of (2.2) would have to use a time step sufficiently small to resolve the gravity waves. This also would imply that the observational system must have sufficient resolution to accurately measure those waves in time and space (which currently is not the case). On the other hand, if there is a dominant component of the solution that is essentially independent of the gravity waves, then gravity waves play only a minor role in the evolution of that solution and need not be accurately observed. Under the assumption that there is a dominant component of the solution of the latter form, Browning and Kreiss (1994a) have proved that the corresponding component of the solution satisfying (2.2) is accurately described by the reduced system

$$\frac{du}{dt} + \rho_0^{-1}p_x - fv = 0, \tag{2.3a}$$

$$\frac{dv}{dt} + \rho_0^{-1}p_y + fu = 0, \tag{2.3b}$$

$$u_x + v_y = F_p, \tag{2.3c}$$

where $d/dt = \partial/\partial t + u\partial/\partial x + v\partial/\partial y + H\partial/\partial z$ and $F_p = -(\gamma p_0 H_z + H p_{0z})/(\gamma p_0)$. In this system vorticity is generated directly from the divergence created by the heating, and gravity waves play no role in the solution. Note that the decomposition of the solution comes from the presence of a large heating term and is not related to the normal modes of a linear version of the system.

The proof showing that the multiscale system for the atmosphere (Browning and Kreiss 1986) accurately describes slowly varying in time mesoscale motions requires that a change of variable be made (see section 3). However, in the particular experimental results obtained during the course of this investigation, the solution was also accurately described by the multiscale system without that change of variable. To better understand how this could occur, an additional scaling will also be considered. For this case the parameters have the values

$$L_1 = L_2 = 100 \text{ km}, \quad D = 10 \text{ km}, \tag{2.4a}$$

$$U = V = 10^{1/2}\,\text{m s}^{-1}, \; W = 10^{-1}\,\text{m s}^{-1}, \; S_1 = 10^{-7/2}, \tag{2.4b}$$

and the corresponding dimensionless system is

$$\frac{ds}{dt} - \epsilon^{-2}\tilde{s}(w - H) = 0, \tag{2.5a}$$

$$\frac{du}{dt} + \epsilon^{-1/2}(\rho_0^{-1}p_x - fv) = 0, \tag{2.5b}$$

$$\frac{dv}{dt} + \epsilon^{-1/2}(\rho_0^{-1}p_y + fu) = 0, \tag{2.5c}$$

$$\frac{dw}{dt} + \epsilon^{-3}(\rho_0^{-1}p_z + \tilde{p}p + gs) = 0, \tag{2.5d}$$

$$\frac{dp}{dt} + \epsilon^{-7/2}wp_{0z} + \epsilon^{-7/2}\gamma p_0(u_x + v_y + \epsilon^{1/2}w_z) = \epsilon^{-2}G, \tag{2.5e}$$

where for this case $d/dt = \partial/\partial t + u\partial/\partial x + v\partial/\partial y + \varepsilon^{1/2}w\partial/\partial z$. The reason for introducing (2.4) is to show what happens with the same horizontal length and vertical depth scales as in (2.1), but with a smaller vertical velocity, that is, a vertical velocity between the one for the large scale and case (2.1). As can be seen in (2.5), the slowly varying solutions in this case must have a small amount of geostrophic balance and a higher degree of hydrostatic balance than for the slowly varying solutions of (2.2). Both of these characteristics were ob-

served in the accurate numerical solution of a model using a heating function typical of those observed in the mesoscale case (e.g., Houze 1989). By studying both scalings, the reason why the multiscale system with and without a change of variable provides accurate solutions is apparent. Note that the dimensional version of the reduced system (2.3) accurately describes the dominant part of the slowly varying solutions for both scalings (and the convective case).

3. Lateral extent of domain and heating of comparable size

Browning and Kreiss (1986) introduced a modification of the Eulerian system of equations describing large-scale atmospheric flows and proved that the modified (multiscale) system accurately describes the slowly varying component of those flows. The selection of appropriate boundary conditions for the modified system ensures that the limited area forecasting problem will be well posed. [The primitive equations do not allow such a selection of boundary conditions; that is, the limited area forecasting problem for the primitive equations is always ill posed (Oliger and Sundström 1978). A similar problem occurs with centered semi-implicit treatments of the unmodified system (Browning and Kreiss 1994b).] The modified system is also able to handle large, medium, and small topographic features (Browning and MacDonald 1993). The Browning and MacDonald paper was the first demonstration of the multiscale nature of the new system. This section contains a proof that the system also accurately describes slowly varying in time mesoscale motions when the lateral extent of the domain and the heating are of comparable size. (No proof is needed for the convective scale because there the modification parameter is one and the system is identical to the unmodified Eulerian equations.)

First consider the dimensionless system (2.2). Assume that the system starts from rest and that the heating is slowly turned on at a later time. As shown previously (Browning and Kreiss 1994a), for slowly varying solutions of (2.2) it must be the case that

$$w = H + \varepsilon^2 w', \tag{3.1}$$

where w' is slowly varying. After making this suggested change of variable, system (2.2) becomes

$$\frac{ds}{dt} - w = 0, \tag{3.2a}$$

$$\frac{du}{dt} + p_x - v = 0, \tag{3.2b}$$

$$\frac{dv}{dt} + p_y + u = 0, \tag{3.2c}$$

$$\frac{dw}{dt} + \epsilon^{-4}(p_z + s) = -\epsilon^{-2}\frac{dH}{dt}, \tag{3.2d}$$

$$\frac{dp}{dt} + \epsilon^{-3}(u_x + v_y + \epsilon^2 w_z) = -\epsilon^{-3}H_z, \tag{3.2e}$$

where $d/dt = \partial/\partial t + u\partial/\partial x + v\partial/\partial y + H\partial/\partial z$ and a number of terms that are not essential to the argument and the prime notation on w have been dropped. This change of variable can be used for all scales of motion without affecting the accuracy of the multiscale system. The multiscale system version of (3.2) is

$$\frac{ds}{dt} - w = 0, \tag{3.3a}$$

$$\frac{du}{dt} + p_x - v = 0, \tag{3.3b}$$

$$\frac{dv}{dt} + p_y + u = 0, \tag{3.3c}$$

$$\frac{dw}{dt} + \alpha\epsilon^{-4}(p_z + s) = 0, \tag{3.3d}$$

$$\frac{dp}{dt} + \epsilon^{-3}(u_x + v_y + \epsilon^2 w_z) = -\epsilon^{-3}H_z, \tag{3.3e}$$

where $d/dt = \partial/\partial t + u\partial/\partial x + v\partial/\partial y + H\partial/\partial z$ and $\alpha = (D/L)^2 = \varepsilon^2$. Note that the term on the right-hand side of (3.2d) is not present in (3.3d) so the vertical derivative of the heating term is the only extra computation in (3.3) compared to (2.2).

System (3.3) can be used to describe the slowly varying solutions of (3.2) up to an error term $O(\varepsilon^2)$. Let a bar over a variable indicate a slowly varying solution of (3.2) and linearize (3.3) about that solution; that is, write the solution of (3.3) as $s = \bar{s} + s'$, $u = \bar{u} + u'$, ···. Ignoring the small nonlinear terms, the linear system describing the deviation (prime) variables is given by

$$\frac{ds'}{dt} - w' = 0, \tag{3.4a}$$

$$\frac{du'}{dt} + p'_x - v' = 0, \tag{3.4b}$$

$$\frac{dv'}{dt} + p'_y + u' = 0, \tag{3.4c}$$

$$\frac{dw'}{dt} + \epsilon^{-2}(p'_z + s') = F, \tag{3.4d}$$

$$\frac{dp'}{dt} + \epsilon^{-3}(u'_x + v'_y + \epsilon^2 w'_z) = 0, \tag{3.4e}$$

where $d/dt = \partial/\partial t + \bar{u}\partial/\partial x + \bar{v}\partial/\partial y + H\partial/\partial z$, $F = -[(1 - \varepsilon^2)d\bar{w}/dt - dH/dt]$, and a number of terms that do not affect the essence of the argument have been dropped. Because systems (3.2) and (3.3) both start from rest and the heating is slowly turned on at a later time, system (3.4) also starts from rest and the difference between the solutions of systems (3.2) and (3.3) is caused only by the forcing F. Thus at first it would seem that the error would be $O(1)$, that is, the same size as the forcing. However, now make the change of variable

$$s' = \varepsilon^2 F + \sigma, \tag{3.5}$$

and transform the resulting system into a symmetric hyperbolic system by rescaling some of the dependent variables to obtain

$$\frac{d(\epsilon\sigma)}{dt} - \epsilon^{-1}(\epsilon^2 w') = -\epsilon^3\frac{dF}{dt}, \quad (3.6a)$$

$$\frac{du'}{dt} + \epsilon^{-3/2}(\epsilon^{3/2}p')_x - v' = 0, \quad (3.6b)$$

$$\frac{dv'}{dt} + \epsilon^{-3/2}(\epsilon^{3/2}p')_y + u' = 0, \quad (3.6c)$$

$$\frac{d(\epsilon^2 w')}{dt} + \epsilon^{-3/2}(\epsilon^{3/2}p')_z + \epsilon^{-1}(\epsilon\sigma) = 0, \quad (3.6d)$$

$$\frac{d(\epsilon^{3/2}p')}{dt} + \epsilon^{-3/2}[u'_x + v'_y + (\epsilon^2 w')_z] = 0. \quad (3.6e)$$

Because $\bar{w}$, H, and all their derivatives are initially zero, from (3.5) this is also true for σ and all its derivatives. Assume periodicity in x and y and rigid walls on the bottom and top of the atmosphere. Then the size of the error is determined solely by the size of the forcing, and standard mathematical energy techniques (e.g., Kreiss and Lorenz 1989) provide the estimate

$$\|(\varepsilon\sigma, u', v', \varepsilon^2 w', \varepsilon^{3/2}p')^T\| \le O(\varepsilon^3) \quad (3.7)$$

and, because all the derivatives of the dependent variables in (3.6) are initially zero, a similar estimate for all spatial and temporal derivatives of the dependent variables in (3.6). From (3.7) it can be seen that $\varepsilon\sigma$, u', and v' are $O(\varepsilon^3)$, and then (3.5) implies $s' = O(\varepsilon^2)$. This is also true for all derivatives of these three quantities. If estimates for w' and p' were obtained directly from (3.7), then the error would appear to be less than $O(\varepsilon^2)$. However, from (3.4a)

$$w' = s'_t + \bar{u}s'_x + \bar{v}s'_y + Hs'_z,$$

and all terms on the right-hand side are $O(\varepsilon^2)$. Using (3.4b–d), the following elliptic equation for the pressure is obtained (Browning and Kreiss 1986):

$$p'_{xx} + p'_{yy} + p'_{zz} = -u'_y + v'_x - s'_z - \left[\left(\frac{du'}{dt}\right)_x + \left(\frac{dv'}{dt}\right)_y + \epsilon^2\left(\frac{dw'}{dt}\right)_z\right] + \epsilon^2 F_z.$$

Because of the chosen value for α, the coefficients of the terms on the left-hand side are all the same size, and because of the estimates obtained earlier, all terms on the right-hand side are $O(\varepsilon^2)$. Thus all derivatives of p' are $O(\varepsilon^2)$. The mean of p' can be obtained by integrating (3.4e) over the spatial domain and is also $O(\varepsilon^2)$. Thus the overall error can be seen to be $O(\varepsilon^2)$ as stated.

Now consider the alternate scaling (2.4). First note that if the change of variable (3.1) is applied, a proof similar to the one above shows that the corresponding multiscale system [which has the same dimensional form as the dimensional version of (3.3)] accurately describes the slowly varying solutions of (2.5). However, in this case it can be shown that the change of variable is not necessary. The multiscale system for the dimensionless system (2.5) is

$$\frac{ds}{dt} - \epsilon^{-2}\tilde{s}(w - H) = 0, \quad (3.8a)$$

$$\frac{du}{dt} + \epsilon^{-1/2}(\rho_0^{-1}p_x - fv) = 0, \quad (3.8b)$$

$$\frac{dv}{dt} + \epsilon^{-1/2}(\rho_0^{-1}p_y + fu) = 0, \quad (3.8c)$$

$$\frac{dw}{dt} + \epsilon^{-1}(\rho_0^{-1}p_z + \tilde{p}p + gs) = 0, \quad (3.8d)$$

$$\frac{dp}{dt} + \epsilon^{-7/2}wp_{0z} + \epsilon^{-7/2}\gamma p_0(u_x + v_y + \epsilon^{1/2}w_z) = \epsilon^{-2}G, \quad (3.8e)$$

where for this case $d/dt = \partial/\partial t + u\partial/\partial x + v\partial/\partial y + \varepsilon^{1/2}w\partial/\partial z$. Using techniques similar to those in the proof of the accuracy of the multiscale system for the large-scale case (Browning and Kreiss 1986), it can be shown that (3.8) describes the slowly varying solutions of (2.5) to within an error term, $O(\varepsilon)$.

4. Lateral extent of domain larger than lateral extent of heating

In the case when the lateral extent of the domain of solution and the heating are comparable, the multiscale system (3.3) has been shown to be able to describe slowly varying solutions of the mesoscale system (3.2) up to an error term, $O(\varepsilon^2)$. Many numerical simulations of mesoscale motions satisfy the hypothesis of the previous section, and the results contained there are applicable to the situations where slowly varying in time gravity waves are very small. However, in reality the domain of solution (the earth) has a much larger lateral extent than that of the heating in a mesoscale storm. It will now be proved that large-scale gravity waves with a timescale similar to the reduced system component of the mesoscale motion and large amplitudes in the pressure can be generated in this case. It will also be shown that the kinetic energy in these waves is small compared to that in the reduced system component of the solution and that the gravity waves are essentially uncoupled from the reduced system component. A technique similar to the one that follows, that is, an analysis of the residual component of the solution after removal of the balanced portion, was used by Ley and Peltier (1978).

To begin the analysis, assume the existence of a large-scale solution (denoted by a bar over the variables) that satisfies the inviscid Eulerian equations with only the large-scale component of the heating included. The mesoscale motion is considered to be a small perturbation

of this large-scale solution. Because the horizontal length scale and the timescale of a large-scale solution are an order of magnitude larger than their mesoscale counterparts, $\bar{u}$ and $\bar{v}$ can be assumed to be independent of x, y, and t. Also, the size of the vertical velocity of the large-scale solution is two orders of magnitude smaller than that arising from the local heating, so the vertical advection terms are dominated by the latter part. Then it is sufficient to consider the linear variable coefficient system

$$\frac{ds}{dt} - w = 0, \tag{4.1a}$$

$$\frac{du}{dt} + p_x - v = 0, \tag{4.1b}$$

$$\frac{dv}{dt} + p_y + u = 0, \tag{4.1c}$$

$$\epsilon^4 \frac{dw}{dt} + p_z + s = -\epsilon^2 \frac{dH}{dt}, \tag{4.1d}$$

$$\epsilon^3 \frac{dp}{dt} + u_x + v_y + \epsilon^2 w_z = -H_z, \tag{4.1e}$$

where $d/dt = \partial/\partial t + \bar{u}(z)\partial/\partial x + \bar{v}(z)\partial/\partial y + H(x, y, z, t)\partial/\partial z$. System (4.1) will be assumed to be applicable in the domain $\{(x, y, z, t) \mid -\infty < x, y < \infty, 0 \le z \le Z, t > 0\}$. To ensure that the linear system has the same solid wall boundary conditions as the large-scale solution at the surface and top of the domain [$\bar{w}(x, y, 0, t) = \bar{w}(x, y, Z, t) = 0$], it will be assumed that $H(x, y, 0, t) = H(x, y, Z, t) = 0$. The system will start from rest and the heating will be assumed to have compact support (the heating is identically zero outside a closed and bounded region) in space and time. Note that then the forcing terms will have compact support in space and time and their derivatives will be $O(1)$ because of the form of their dependence on the heating and the large-scale solution.

A direct application of the mathematical energy method to (4.1) leads to poor estimates because of the skewing in the system (Browning and Kreiss 1994b). Therefore, the analysis of system (4.1) will be performed by expanding its slowly varying solution in terms of solutions of a number of reduced systems and one additional system that describes the gravity waves. The easiest way to obtain estimates for the reduced system for the mesoscale case is to assume that the vertical advection terms are not present; that is, to consider the reduced system for the external mode shallow water equations, and then to expand the solution of the reduced system for the mesoscale case in terms of solutions of the reduced system for the external mode shallow water equations. When this is done, forcing terms due to the neglect of the vertical advection terms will appear in the equations that describe the residual component of the solution. Thus the first step in the analysis is to estimate the solutions for the reduced system (2.3) when there are forcing terms in the momentum equations.

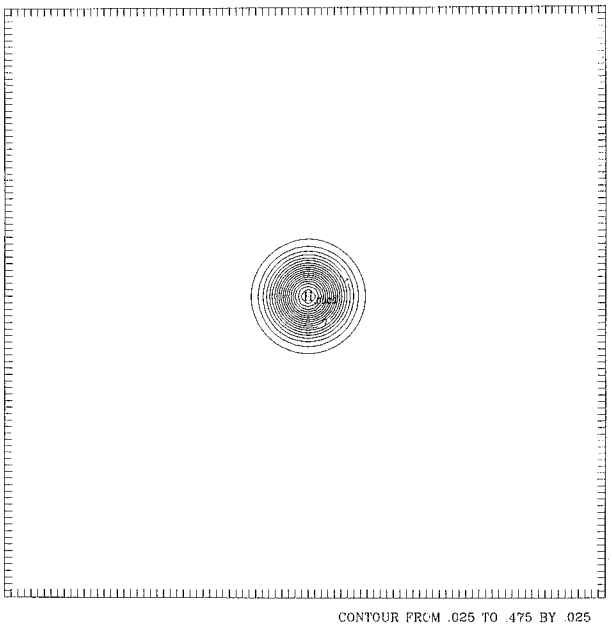

FIG. 1. The spatial component of the heating $H_0H_1H_2$ at $z = 9$ km. The contour interval is 0.025 m s^{-1}.

Lemma 1. Consider the system

$$\frac{du}{dt} + p_x - v = G_1, \tag{4.2a}$$

$$\frac{dv}{dt} + p_y + u = G_2, \tag{4.2b}$$

$$u_x + v_y = 0, \tag{4.2c}$$

where $d/dt = \partial/\partial t + \bar{u}(z)\partial/\partial x + \bar{v}(z)\partial/\partial y + H(x, y, z, t)\partial/\partial z$, G_1 and G_2 and all their derivatives belong to L_2, and $u(x, y, z, 0) = v(x, y, z, 0) = 0$. Then u, v, p_x, p_y, and their derivatives with respect to x, y, z, and t belong to L_2 and can be estimated in terms of G_1, G_2, and their derivatives.

Proof. The mathematical energy method can be applied to (4.2) to obtain estimates for u and v in terms of G_1 and G_2. Estimates of the derivatives of u and v can be obtained by appropriately differentiating (4.2). Then estimates for p_x and p_y and their derivatives can be obtained from the appropriate derivatives of (4.2a) and (4.2b).

Note that lemma 1 does not provide estimates for p. With an additional assumption on the nature of the forcing in (4.2), estimates for p can also be obtained.

Lemma 2. Consider system (4.2) and also assume that G_1 and G_2 have compact support. Denote by $\hat{p}$ the Fourier transform of p:

$$\hat{p}(\underline{\omega}, t) = \int e^{i(\underline{\omega}, \mathbf{x})} p(\mathbf{x}, t)\, d\mathbf{x},$$

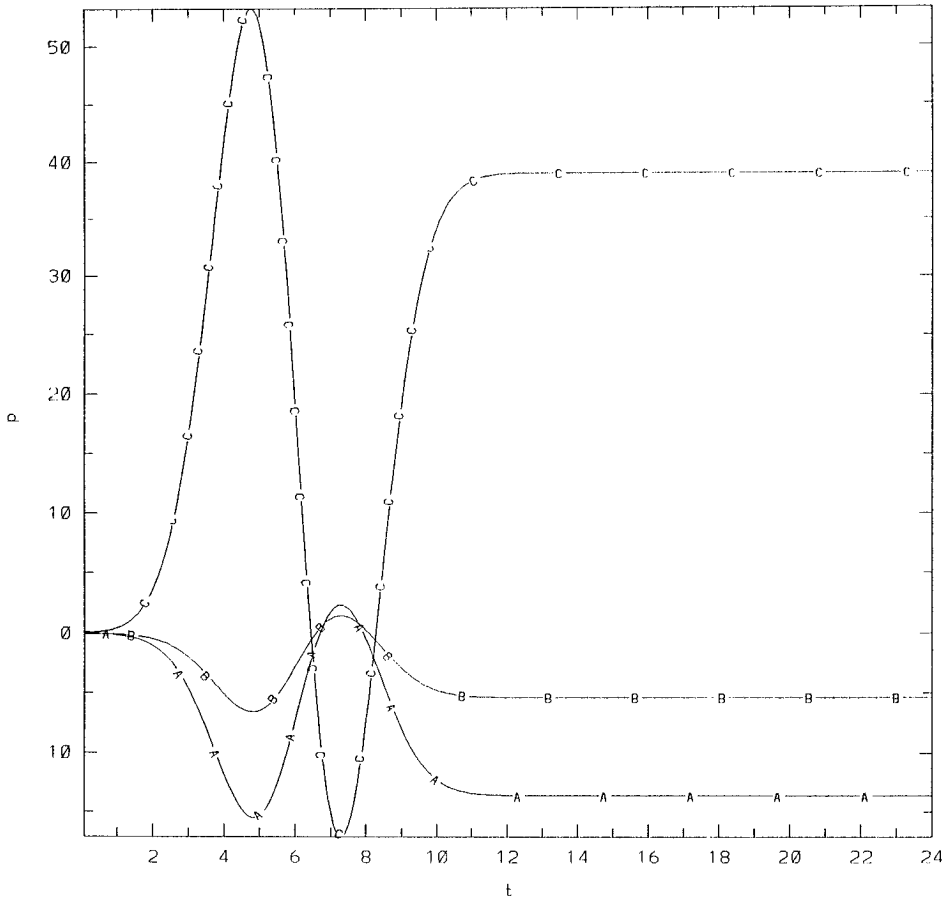

FIG. 2. The geopotential ($m^2\ s^{-2}$) from the reduced system model plotted at the grid points $A = (0, 0, 0)$, $B = (20, 20, 0)$, and $C = (40, 40, 0)$ as a function of time (h).

where $\mathbf{x} = (x, y)^T$ and $\underline{\omega} = (\omega_1, \omega_2)^T$ is the real dual variable of $\mathbf{x}$. Then $\hat{p}$ vanishes rapidly for $\omega \to \infty$. Also, $\hat{p}$ is of the form

$$\hat{p}(\underline{\omega}, t) = |\underline{\omega}|^{-2} p_1(\underline{\omega}, t),$$

where $\hat{p}_1(\underline{\omega}, t)$ is a smooth function of $\underline{\omega}$ with $\hat{p}_1(0, t) = 0$; that is, $|\hat{p}| = \text{const.}|\underline{\omega}|^{-1}$. Let

$$\hat{q} = |\underline{\omega}|^{-1} \hat{p}_1(\underline{\omega}),$$

and denote by q the corresponding function in physical space. The norm of q and its derivatives can be estimated in terms of the norms of G_1, G_2, and their derivatives.

Proof. The vertical component of the vorticity is $\zeta \equiv -u_y + v_x$. Differentiating the momentum equations appropriately and then adding them together gives

$$\zeta_t + \bar{u}\zeta_x + \bar{v}\zeta_y - (Hu_z - G_1)_y + (Hv_z - G_2)_x = 0.$$

Therefore, ζ has compact support in every finite time interval and $\hat{\zeta}(\underline{\omega}, t)$ is a smooth function of $\underline{\omega}$. Also,

$$\frac{\partial}{\partial t} \int \zeta \, d\mathbf{x} = 0, \qquad \text{that is,} \qquad \int \zeta \, d\mathbf{x} = 0$$

implies that

$$\hat{\zeta}(0, t) = 0.$$

The pressure equation has the form

$$\nabla^2 p - \zeta + (Hu_z - G_1)_x + (Hv_z - G_2)_y = 0,$$

and Fourier transforming the last equation provides the stated information about p.

Now the issue of the forcing term in (2.3c) will be considered. The main problem here is that when there is a forcing term, it must satisfy an integral constraint because the left-hand side is the divergence of the velocity. This constraint is not satisfied by a general heating function, so that function has to be partitioned into two parts: one that satisfies the constraint and one that does not (it is exactly the latter part of the heating that gives rise to the gravity waves). Here estimates will be obtained for the component of the solution corresponding to the component of forcing that satisfies the constraint. (As mentioned earlier, initially estimates are obtained for a simpler case where the vertical advection terms are neglected.)

Lemma 3. Consider the constant coefficient system

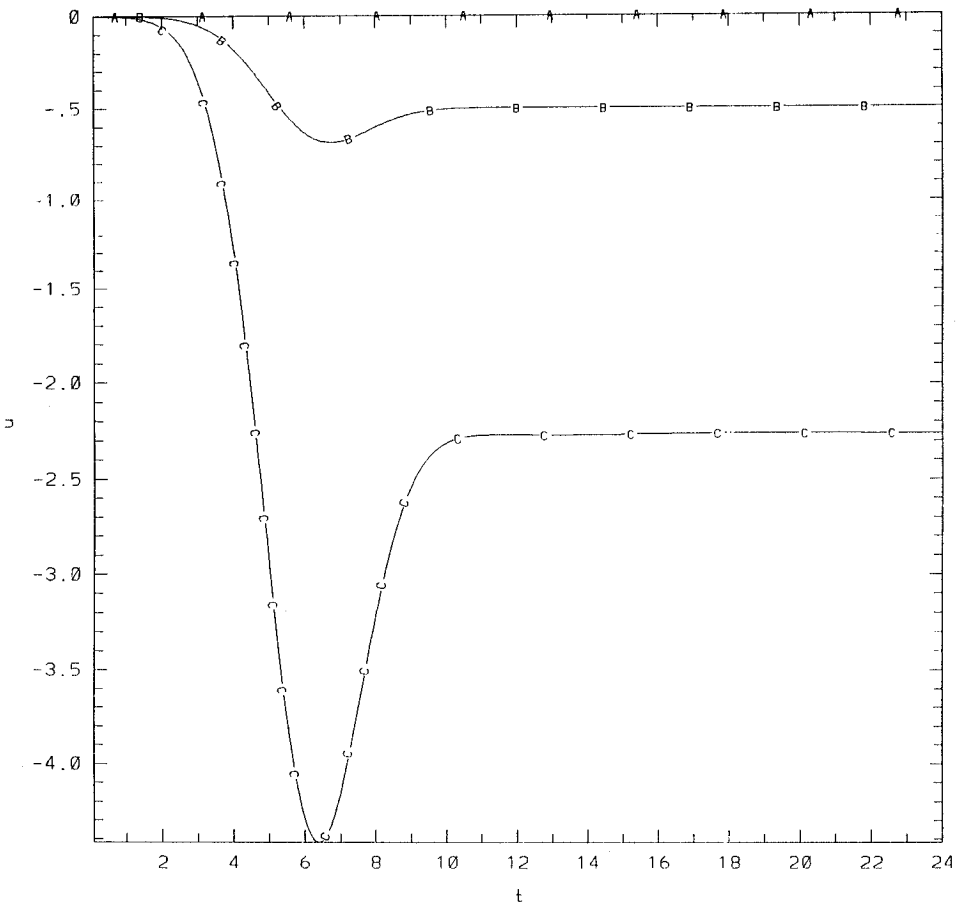

FIG. 3. The eastward component of the velocity (m s^{-1}) from the reduced system model plotted at the same grid points as in Fig. 2 as a function of time (h).

$$\frac{d_H u}{dt} + p_x - v = 0, \tag{4.3a}$$

$$\frac{d_H v}{dt} + p_y + u = 0, \tag{4.3b}$$

$$u_x + v_y = G, \qquad \int G\, d\mathbf{x} = 0, \tag{4.3c}$$

where

$$\frac{d_H}{dt} = \frac{\partial}{\partial t} + \bar{u}\frac{\partial}{\partial x} + \bar{v}\frac{\partial}{\partial y}.$$

Assume that G and all its derivatives belong to L_2 and that $|\underline{\omega}|^{-1}\hat{G}(\underline{\omega}, t)$ is bounded. Then u, v, p_x, p_y, and all their derivatives can be estimated in terms of $\|d^j G/dx^j\|$, $\|d^j G/dy^j\|$, and $|\underline{\omega}|^{-1}|\hat{G}(\underline{\omega}, t)|$.

Proof. The vorticity equation for this case is

$$\frac{d_H \zeta}{dt} = -G \quad \text{or} \quad \hat{\zeta} + (\bar{u} i\omega_1 + \bar{v} i\omega_2)\hat{\zeta} = -\hat{G}.$$

Therefore $\hat{\zeta}$ can be estimated in terms of $\hat{G}$. From the Helmholtz relations

$$\nabla^2 u = -\zeta_y, \quad \text{i.e.,} \quad \hat{u} = \text{const} \times i\omega_2 |\omega|^{-2}\hat{G},$$

and, therefore, $\hat{u}$ can be estimated in terms of $|\underline{\omega}|^{-1}\hat{G}(\underline{\omega}, t)$ The pressure equation

$$\nabla^2 p = \zeta - \frac{d_H G}{dt}, \quad \text{i.e.,} \quad \hat{p} = |\omega|^{-2}\left(\zeta - \frac{d_H \hat{G}}{dt}\right)$$

gives the estimates for the derivatives of p.

Now it is possible to use Lemmas 1 and 3 to estimate the solution of the reduced system with the vertical advection terms included.

Lemma 4. Consider the system

$$\frac{du}{dt} + p_x - v = 0, \tag{4.4a}$$

$$\frac{dv}{dt} + p_y + u = 0, \tag{4.4b}$$

$$u_x + v_y = G, \tag{4.4c}$$

where G has the properties of Lemma 3. The solution can be estimated in the same way as in Lemma 3.

Proof. Solve system (4.3) and denote the solution by

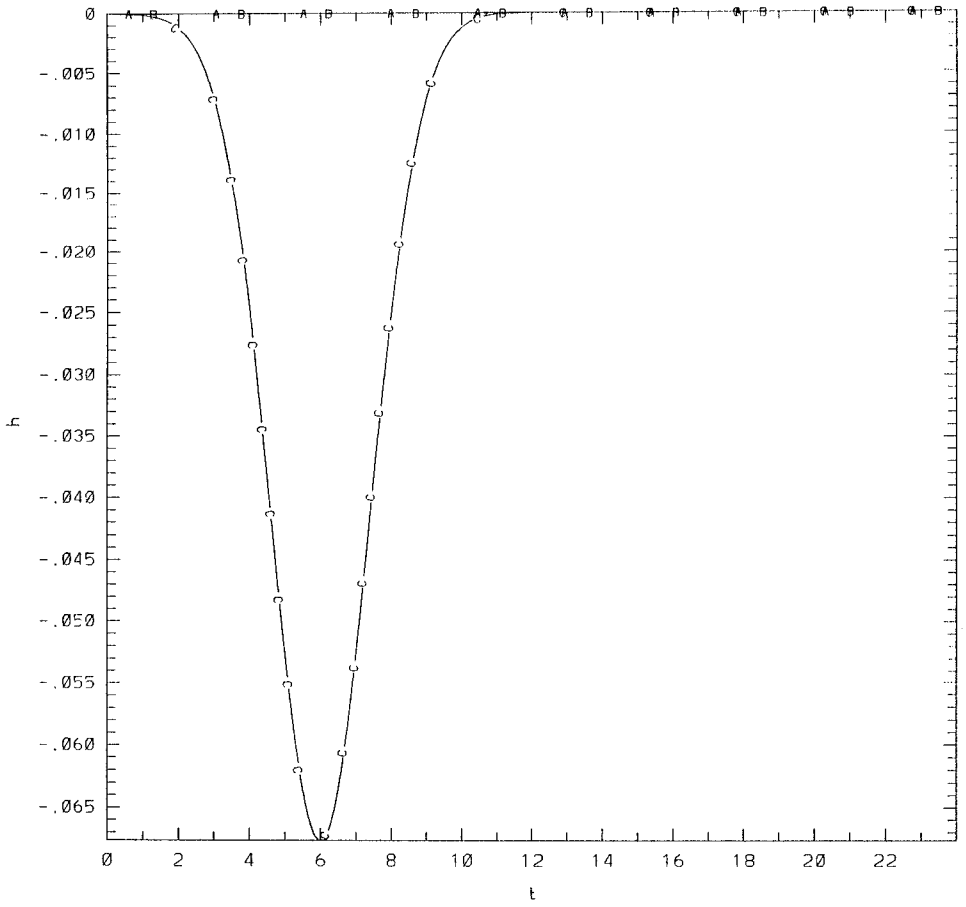

FIG. 4. The vertical velocity (m s^{-1}) from the reduced system model plotted at the grid points $A = (0, 0, 3)$, $B = (20, 20, 3)$, and $C = (40, 40, 3)$ as a function of time (h).

$u^{(1)}, \cdots$. The differences between that solution and the solution of (4.4), that is, $u^{(2)} = u - u^{(1)}, \cdots$, satisfy (4.2) with

$$G_1 = Hu_z^{(1)},\ G_2 = Hv_z^{(1)}.$$

Because H has compact support, Lemma 1 can be used to complete the estimate.

Now the part of the forcing $-H_z$ that does not satisfy the integral constraint, that is, the portion of the spectrum of the forcing near the origin, must be considered. Clearly the corresponding part of the mesoscale solution cannot be described by the reduced system, and it is exactly this part of the heating that gives rise to large-scale gravity waves. [When the lateral extent of the domain is finite, only the mean of the forcing F_p must be zero to satisfy the constraint arising from Eq. (2.3c) of the reduced system. For the finite domain case, it has been rigorously proved that the interaction of the gravity waves with the dominant component of the solution is minimal (Kreiss et al. 1991).]

Lemma 5. Let G be a function whose transform satisfies $\hat{G}(\underline{\omega}, t) = 0$ for $|\underline{\omega}| \geq K\varepsilon$ and consider the system

$$\frac{d_H s}{dt} - w = 0, \tag{4.5a}$$

$$\frac{d_H u}{dt} + p_x - v = 0, \tag{4.5b}$$

$$\frac{d_H v}{dt} + p_y + u = 0, \tag{4.5c}$$

$$\epsilon^4 \frac{d_H w}{dt} + p_z + s = 0, \tag{4.5d}$$

$$\epsilon^3 \frac{d_H p}{dt} + u_x + v_y + \epsilon^2 w_z = G. \tag{4.5e}$$

The limit on the support of $\hat{G}$ is determined by the following considerations. After one step of the expansion procedure for the solution of the full system (4.1), if K is sufficiently large, the forcing terms will all be reduced by an order of magnitude. Then the procedure can be repeated until the forcing terms are sufficiently small so that even the poor estimates obtained from the energy method for the badly skewed system are ade-

quate to show that the difference between the solution of (4.1) and the expansion remains small.

The solution of system (4.5) can be calculated explicitly and consists of large-scale gravity waves with the same timescale as the reduced system component of the solution.

Proof. It is possible to obtain an estimate of G that is proportional to the area of the rectangle of the support of $\hat{G}$. Let $x = \varepsilon\tilde{x}$. From the definition of the Fourier transform

$$\begin{aligned} G &= \int_{|\omega_j| \le K\epsilon} e^{i(\omega,\mathbf{x})}\hat{G}(\omega, t)\, d\omega \\ &= \int_{|\omega_j| \le K\epsilon} e^{i(\epsilon^{-1}\omega,\epsilon\mathbf{x})}\hat{G}(\omega, t)\, d\omega \\ &= \epsilon^2 \int_{|\tilde{\omega}_j| \le K} e^{i(\tilde{\omega},\tilde{\mathbf{x}})}\hat{G}(\epsilon\tilde{\omega}, t)\, d\tilde{\omega} \\ &\approx \epsilon^2\hat{G}(0, t)\int_{|\tilde{\omega}_j| \le K} e^{i(\tilde{\omega},\tilde{\mathbf{x}})}\, d\tilde{\omega} \\ &= \epsilon^2\hat{G}(0, t)(\tilde{x}\tilde{y})^{-1}\sin K\tilde{x}\,\sin K\tilde{y}. \end{aligned} \tag{4.6}$$

Because G is a slowly varying function of $\tilde{\mathbf{x}}$, the solution of (4.5) is also a slowly varying function of $\tilde{\mathbf{x}}$. Therefore the change of independent variable $\tilde{\mathbf{x}} = \varepsilon\mathbf{x}$ in (4.5) is appropriate. Also, to transform the system into a symmetric hyperbolic system, the change of dependent variable $\tilde{p} = \varepsilon^{3/2}p$ is necessary. Then (4.5) becomes

$$s_t - w = 0, \tag{4.7a}$$

$$u_t + \epsilon^{-1/2}\tilde{p}_{\tilde{x}} - v = 0, \tag{4.7b}$$

$$v_t + \epsilon^{-1/2}\tilde{p}_{\tilde{y}} + u = 0, \tag{4.7c}$$

$$\tilde{p}_z + \epsilon^{3/2}s = 0, \tag{4.7d}$$

$$\tilde{p}_t + \epsilon^{-1/2}[u_{\tilde{x}} + v_{\tilde{y}}] + \epsilon^{1/2}w_z = \epsilon^{-3/2}G. \tag{4.7e}$$

After the transformation of the spatial variables, the horizontal advection terms are small and can be neglected. The resulting constant coefficient system can be solved explicitly. Differentiating (4.7e) with respect to t and then using (4.7a–d), the gravity wave equation for $\tilde{p}$ is

$$(-D_z^2 + \epsilon)\tilde{p}_{tt} - (\tilde{p}_{\tilde{x}\tilde{x}} + \tilde{p}_{\tilde{y}\tilde{y}}) + \epsilon^{1/2}(-u_{\tilde{y}} + v_{\tilde{x}}) = \epsilon^{-1/2}G_t.$$

Note that the forcing of the gravity waves by the vorticity plays a secondary role relative to the heating (e.g., Ford 1994). Using (4.6), in this scaling gravity waves with amplitudes $O(\varepsilon^{3/2})$ are generated. In the original variables the amplitude of p is $O(1)$, which is the same size as the pressure from the reduced system component of the solution (but of a larger horizontal length scale). On the other hand, the amplitudes of u and v are $O(\varepsilon)$, which is smaller than the velocities in the reduced system component of the solution. Thus, neglecting the gravity wave component of the solution can result in a 100% error in the pressure (in the long waves) but only a 10% error in the velocity. Because the wavelength is $O(\varepsilon^{-1})$, the L_2-norm of these gravity waves is $O(1)$. However, this is still very small compared with the energy in the large scale, which is proportional to the area of the full domain. This portion of the slowly varying in time solution will be called the gravity wave component, for obvious reasons.

Now the above lemmas can be used to approximate the solution of the full system,

$$\frac{ds}{dt} - w = G_1, \tag{4.8a}$$

$$\frac{du}{dt} + p_x - v = G_2, \tag{4.8b}$$

$$\frac{dv}{dt} + p_y + u = G_3, \tag{4.8c}$$

$$\epsilon^4\frac{dw}{dt} + p_z + s = G_4, \tag{4.8d}$$

$$\epsilon^3\frac{dp}{dt} + u_x + v_y + \epsilon^2 w_z = G_5, \tag{4.8e}$$

with homogeneous initial data. The G_j are functions that are slowly varying and have compact support and whose time derivatives vanish at $t = 0$. The solution of (4.8) will be expressed in terms of the simpler systems developed earlier. First solve the reduced system

$$\frac{ds^{(1)}}{dt} - w^{(1)} = G_1, \tag{4.9a}$$

$$\frac{du^{(1)}}{dt} + p_x^{(1)} - v^{(1)} = G_2, \tag{4.9b}$$

$$\frac{dv^{(1)}}{dt} + p_y^{(1)} + u^{(1)} = G_3, \tag{4.9c}$$

$$p_z^{(1)} + s^{(1)} = G_4, \tag{4.9d}$$

$$u_x^{(1)} + v_y^{(1)} = 0. \tag{4.9e}$$

Note that (4.9b), (4.9c), and (4.9e) uncouple and satisfy the hypotheses of Lemma 1. The remaining variables can be obtained from the solution of the uncoupled system using (4.9a) and (4.9d).

The differences $u^{(2)} = u - u^{(1)}$, $\cdots$ satisfy (4.8) with G_1, G_2, G_3, G_4, and G_5 replaced by 0, 0, 0, $G_4^{(1)} = -\varepsilon^4 dw^{(1)}/dt$, and $G_5^{(1)} = G_5 + \varepsilon^3 dp^{(1)}/dt + \varepsilon^2 w_z^{(1)}$, respectively. Repeating the process, $G_4^{(2)} = O(\varepsilon^8)$ and therefore $G_4^{(1)}$ can be replaced by 0. Let $\hat{G}_5^{(1)}$ denote the Fourier transform of $G_5^{(1)}$. Split $\hat{G}_5^{(1)}$ into two pieces, $\hat{G}_5^{(1)} = \hat{R}^I + \hat{R}^{II}$, where R^I contains the spectrum of $G_5^{(1)}$ near the origin and R^{II} contains the rest of the spectrum of $G_5^{(1)}$:

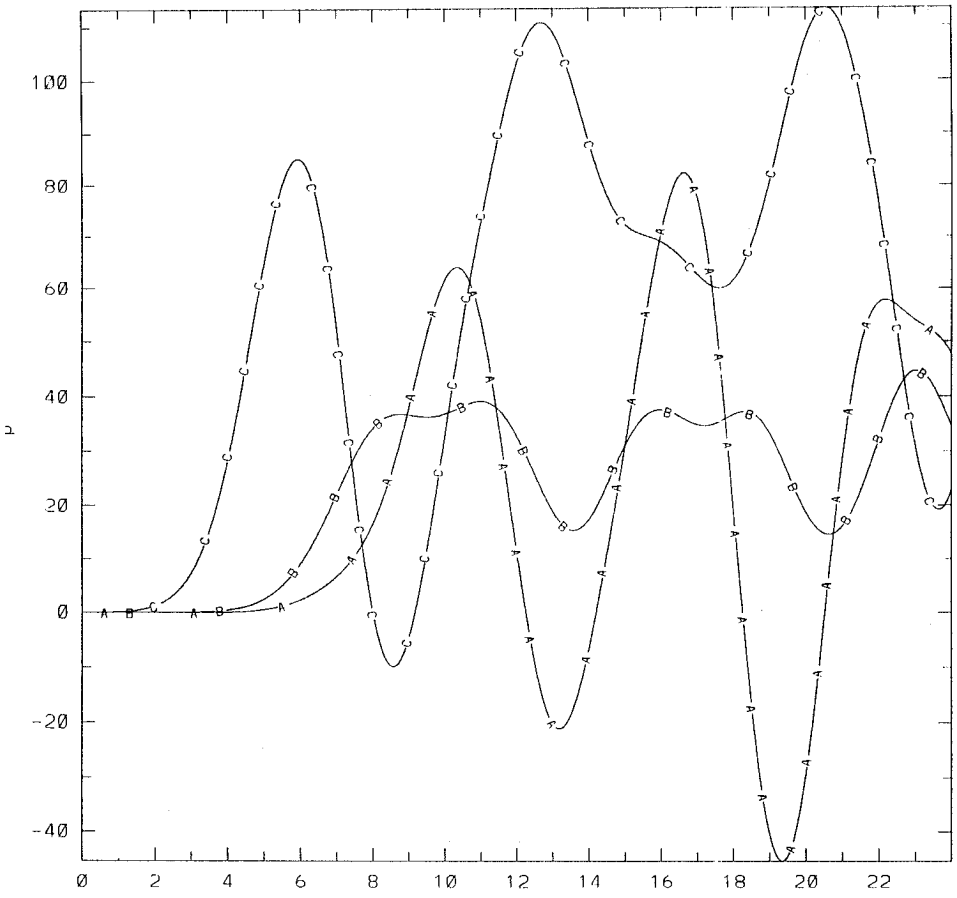

FIG. 5. The geopotential ($m^2\ s^{-2}$) from the full system model plotted at the same grid points as in Fig. 2 as a function of time (h).

$$\hat{R}^I = \begin{cases} \hat{G}_5^{(1)} & \text{for } |\omega_j| \le K\epsilon,\ j = 1, 2 \\ 0 & \text{otherwise,} \end{cases} \quad \hat{R}^{II} = \hat{G}_5^{(1)} - \hat{R}^I.$$

Now solve the gravity wave system (4.5) with $G = R^I$, denote the solution by $u^{(2)}$, $\cdots$ and subtract it from from $u^{(1)}$, $\cdots$. The difference satisfies system (4.8) with $G_1^{(2)} = Hs_z^{(2)}$, $G_2^{(2)} = Hu_z^{(2)}$, $G_3^{(2)} = Hv_z^{(2)}$, $G_4^{(2)} = \varepsilon^4 Hw_z^{(2)}$, and $G_5^{(2)} = R^{II} + \varepsilon^3 Hp_z^{(2)}$. Because H is of compact support, using the same technique as above, it is possible to reduce G_1, G_2, G_3, and G_4 to zero and G_5 to R^{II}. Now solve the reduced system

$$\frac{ds^{(3)}}{dt} - w^{(3)} = 0, \tag{4.10a}$$

$$\frac{du^{(3)}}{dt} + p_x^{(3)} - v^{(3)} = 0, \tag{4.10b}$$

$$\frac{dv^{(3)}}{dt} + p_y^{(3)} + u^{(3)} = 0, \tag{4.10c}$$

$$p_z^{(3)} + s^{(3)} = 0, \tag{4.10d}$$

$$u_x^{(3)} + v_y^{(3)} = R^{II}. \tag{4.10e}$$

The solution of (4.10) can be estimated from Lemma 4. Subtracting it from $u^{(2)}$, $\cdots$, the differences satisfy system (4.8) with a forcing term in (4.8d) of order $O(\varepsilon^4)$ (which can be reduced even further) and a forcing term in (4.8e) of order $O(\varepsilon^2)$; that is, the original forcing in the pressure equation has been reduced by two orders of magnitude.

A summary of the above analysis is that the slowly varying mesoscale solution consists of a component that is accurately described by the reduced system plus a component that is accurately described by the gravity wave equation, and the two components are essentially independent of each other. The pressure perturbations of the two components have the same periods and amplitudes and can be distinguished only by their spatial variation. The kinetic energy in the gravity wave component is much less than in the component that can be expanded in terms of the reduced system.

The proof above can also be applied to the multiscale system. The reduced and gravity wave systems are essentially the same for the unmodified and multiscale systems; that is, they are only slightly less accurate in the latter case because the neglect of the vertical acceleration results in an error of $O(\varepsilon^2)$ instead of an error of $O(\varepsilon^4)$. Because the equation for the large-scale grav-

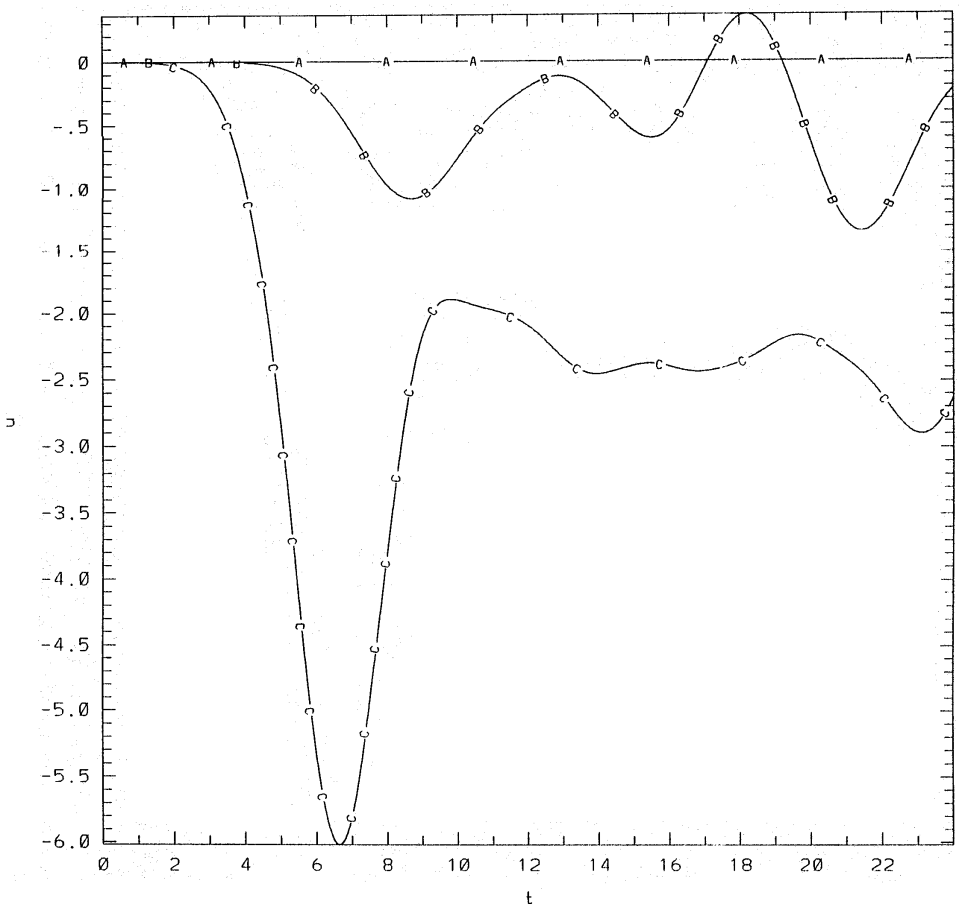

FIG. 6. The eastward component of the velocity (m s^{-1}) from the full system model plotted at the same grid points as in Fig. 2 as a function of time (h).

ity waves is essentially the same in both systems (also see Browning and Kreiss 1985), they are accurately computed by the multiscale system. This will be demonstrated in the following section.

5. Numerical examples

A number of the theoretical results in the previous sections can be demonstrated by specifying a heating function $H(x, y, z, t)$ that has spatial and temporal distributions similar to those observed in the atmosphere. In particular, choose $H = H_0H_1(x, y)H_2(z)H_3(t)$, where

$$H_0 = .5 \text{ m s}^{-1}, \tag{5.1a}$$

$$H_1(x, y) = e^{-[(x-L/2)^2+(y-L/2)^2]/r_e^2},$$

$$r_e = 50 \times 10^3 \text{ m}, \tag{5.1b}$$

$$H_2(z) = \sin(2\pi z/D), \tag{5.1c}$$

$$H_3(t) = e^{-(t-6\times3600)^2/(2\times3600)^2}, \tag{5.1d}$$

$L = 900 \times 10^3$ m is the length and width of the domain, and $D = 12 \times 10^3$ m is the depth. The spatial component of the heating $H_0H_1H_2$ (m s^{-1}) at $z = 9$ km is shown in Fig. 1 and should be compared with the stratiform rain region of Houze's schematic of a typical mesoscale convective system (MCS) (Houze 1989, Fig. 1). Houze shows a domain of length and width 447×10^3 m, a depth of the MCS around 12×10^3 m, a width of the heating of 126×10^3m, and cooling and heating in the lower and upper part of the storm, respectively. This description of the cooling and heating is in close agreement with that given in (5.1). Here the size of the domain is intentionally chosen to be considerably larger than that of the heating to allow the gravity waves to behave more as they would in the real atmosphere. Houze states that the magnitude of the vertical velocity in a wide range of MCSs is on the order of 0.1–0.5 m s^{-1}. From (3.1), the maximum vertical velocity is determined by the maximum value of H and from (5.1a) that will be 0.5 m s^{-1}. Houze does not mention a typical timescale for the storms. This is not surprising because there is considerable variability in the duration of these storms. The time dependence of the heating (5.1d) is a Gaussian distribution centered at 6 h with an e-folding parameter of 2 h. The storm essentially is created in 3 h and dissipates in 3 h; that is, the storm is on the lower end of

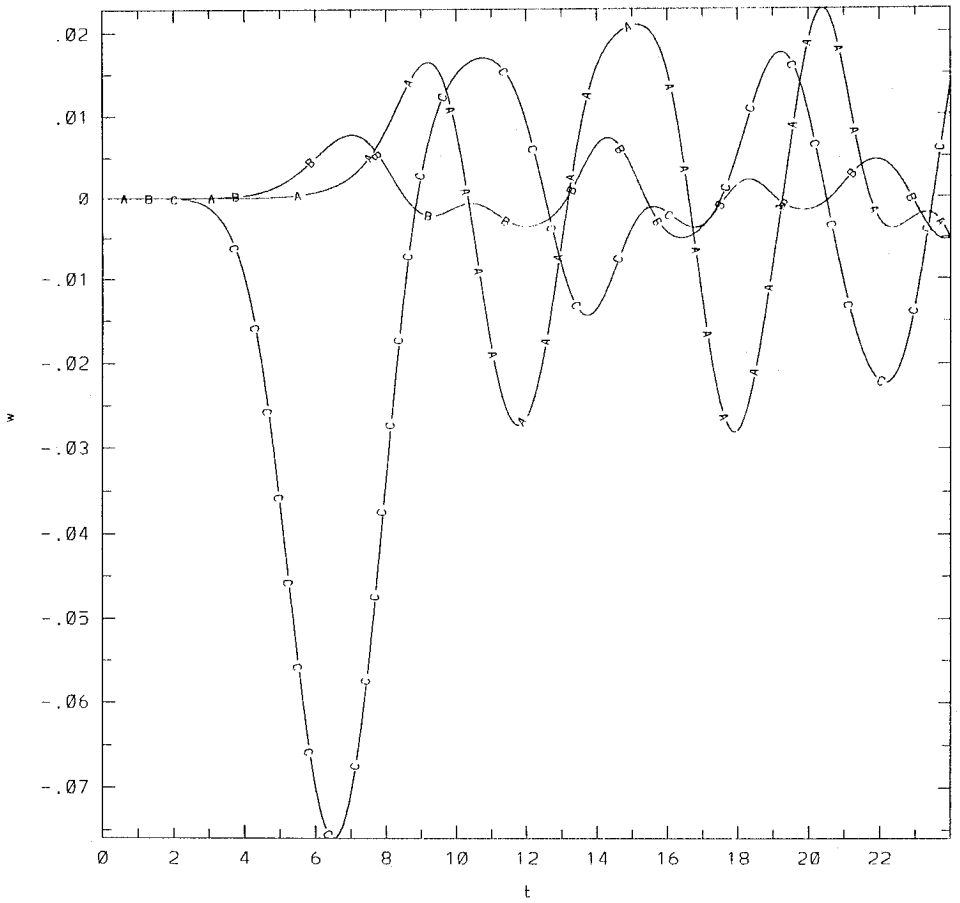

FIG. 7. The vertical velocity (m s^{-1}) from the full system model plotted at the same grid points as in Fig. 4 as a function of time (h).

the typical lifetime of a MCS. [Similar results have been obtained for a convective tower in isolation and in combination with the stratiform heating in (5.1) and for a 50 km by 150 km elliptical heating with a 90-min period (Ralph et al. 1993).]

In order to compare the two components of the solution described in the previous section, it is first necessary to compute a solution of the reduced system (2.3). Most observational studies of gravity waves use surface pressure observations alone or in combination with profiler winds (Ralph et al. 1993). The reduced system will be solved at $z = 0$ to illustrate what surface pressure observations would show. Note that at the surface the vertical advection terms can be dropped because $H(x, y, 0, t) = 0$. Consider (2.3) at the surface of the domain described above with the solution L periodic in x and y. (The heating is not truly periodic, but dies off sufficiently fast to be effectively periodic.) The solution of system (2.3) with the heating (5.1) cannot be obtained analytically, but a numerical model can be used to accurately compute the solution during the lifetime of the storm. To describe the numerical approximation of (2.3) (and of other systems to follow), consider the finite difference grid $G = \{i\Delta x, j\Delta y, k\Delta z, n\Delta t: 0 \le i, \le I, 0 \le j \le J, 0 \le k \le K, n \ge -1\}$, where I, J ($J = I$), and K are the number of grid intervals in the x, y, and z directions, respectively; Δx, Δy, and Δz are the corresponding grid increments; and Δt is the time step. The standard notation $u^n_{i,j,k}$ is used to denote the value of a grid function at the point (x_i, y_j, z_k, t_n) and missing subscripts or superscripts imply the nominal value of the missing variable. Define the finite difference operators

$$D_d \equiv (T_{+d} - T_{-d})/(2\Delta d), \tag{5.2a}$$

$$D_{dd} \equiv (T_{+d} - 2I + T_{-d})/(\Delta d^2), \tag{5.2b}$$

where T_{+d} and T_{-d} (d can be either x, y, z, or t) are the standard forward and backward translation operators along the d axis. The centered second-order finite difference approximation of (2.3) is given by

$$D_t u + uD_x u + vD_y u + D_x(\rho_0^{-1}p) - fv = 0, \tag{5.3a}$$

$$D_t v + uD_x v + vD_y v + D_y(\rho_0^{-1}p) + fu = 0, \tag{5.3b}$$

$$(D_{xx} + D_{yy})(\rho_0^{-1}p) = \tag{5.3c}$$
$$f(-D_y u + D_x v) + 2(D_x u \cdot D_y v - D_y u \cdot D_x v)$$
$$+ \left(\frac{\partial}{\partial t} + u\frac{\partial}{\partial x} + v\frac{\partial}{\partial y}\right)H_z - H_z^2,$$

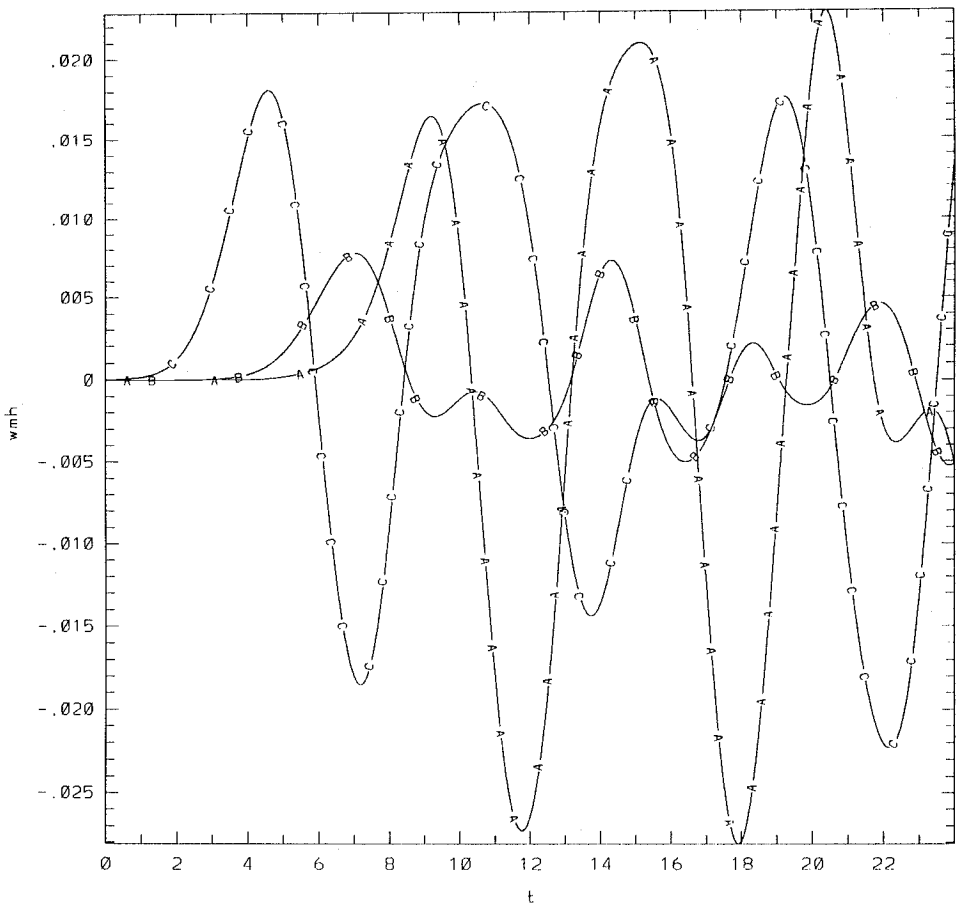

FIG. 8. The difference of the vertical velocities (m s^{-1}) from the full and reduced system models, that is, Fig. 7 minus Fig. 4, plotted at the same grid points as in Fig. 4 as a function of time (h).

where $f = 10^{-4}$ s^{-1}, variables with out-of-range indices can be determined from the periodicity condition, and the equation for pressure can be solved by any standard elliptic solver. Because of the assumption of periodicity, the mean of the pressure on each horizontal level is not determined by (5.3c). However, the mean of the pressure is not needed in the reduced system so it is arbitrarily set to zero. (It is possible to derive an equation for the mean of the pressure following the discussion in section 3, but for our purposes the above technique will suffice.) If the values of the grid functions at $n = -1$ and $n = 0$ are known, then (5.3) can be used to consecutively determine the values of the grid functions at $n > 0$. The solution of (5.3) was computed with adequate numerical resolution ($I = J = 90$ and $\Delta t = 300$ s) to produce an approximation of the solution of (2.3) with H given by (5.1) that was sufficiently accurate for the discussions to follow.

Figures 2 and 3 are plots of the reduced system geopotential p/ρ (m^2 s^{-2}) and eastward component of the wind (m s^{-1}) at the three grid points with indices $A = (0, 0, 0)$, $B = (20, 20, 0)$, $C = (40, 40, 0)$ as a function of time. Point A is at the lower left corner of the domain (as far away from the storm as possible), point B is approximately halfway along the line from point A to the center point of this level, and point C is on the same line near the center of the storm. (Point C was chosen slightly off the center of the storm because $u \equiv 0$ at the center of the storm.) Note that the pressure at point C increases as the storm intensifies and then decreases as the storm diminishes. Thus, if the storm is being advected by the mean wind, the pressure at the surface will increase as the storm passes overhead and then decrease once the storm moves on. All the pressures have a period roughly the same as the period of the heating (≈6–7 h) as might be expected from (2.3) and eventually reach a steady state because the circular heating leaves a circular vortex of the same scale as the heating after it recedes. Figure 4 shows the temporal evolution of the vertical velocity (m s^{-1}) at the same horizontal locations as in Figs. 2 and 3, but at $z = 3$ km (because $w = 0$ at the surface). The vertical velocity in the storm increases in magnitude as the storm intensifies and decreases in magnitude as the storm diminishes as expected from the relation $w = H$.

The next step is to compute the complete solution of

the full system (2.2) so that the difference between this solution and the reduced system solution can be computed to show the residual component, which is dominated by the gravity waves. Consider the dimensional form of system (2.2) in the domain described above with the solution L periodic in x and y. As in the reduced system case, the solution of (2.2) will be obtained by numerical methods. The centered second-order finite difference approximation of the dimensional form of (2.2) (with $G = 0$) is given by

$$D_t s + uD_x s + vD_y s + wD_z s - \tilde{s}(w - H) = 0, \tag{5.4a}$$

$$D_t u + uD_x u + vD_y u + wD_z u + \rho_0^{-1} D_x p - fv = 0, \tag{5.4b}$$

$$D_t v + uD_x v + vD_y v + wD_z v + \rho_0^{-1} D_y p + fu = 0, \tag{5.4c}$$

$$D_t w + uD_x w + vD_y w + wD_z w + \rho_0^{-1} D_z p + \tilde{p}p + gs = 0, \tag{5.4d}$$

$$D_t p + uD_x p + vD_y p + wD_z p + wp_{0z} + \gamma p_0 (D_x u + D_y v + D_z w) = 0, \tag{5.4e}$$

where the mean state quantities $\tilde{s}$, ρ_0, $\tilde{p}$, and p_0 are computed from an isothermal atmosphere whose temperature is 340 K. The numerical approximation of the solution of (2.2) can then be computed in a manner similar to that used for (5.3). The solution of (5.4) was computed with adequate numerical resolution ($I = J = 90$, $K = 12$, and $\Delta t = 2$ s) to produce an approximation of the solution of (2.2) with H given by (5.1) that was sufficiently accurate for the discussions to follow.

To show that the reduced system accurately describes the dominant portion of the solution, the differences between the horizontal velocities for (5.4) and those for (5.3) were computed with the velocities of (5.4) considered to be correct. After the cooling or heating has disappeared ($t \geq 12$ h), there is divergence present in the full system model because of the gravity waves. The magnitude of the vertical velocity (and therefore of the horizontal divergence) of the dominant portion of the solution increases and then decreases to follow the cooling or heating (see 2.3). Once the cooling or heating has disappeared, the vertical velocities that remain are mainly due to the gravity waves. The magnitude of the vertical velocity in these waves is sufficiently small at this point that the dominant portion of the solution is accurately described by the barotropic vorticity equation on each horizontal layer (Browning and Kreiss 1986). The divergent component of the velocity was removed from the wind at the end of the full system model run, using the Helmholtz relations as in an earlier study (Browning and Kreiss 1994a). The relative l_2 error in the velocity at 12 h (a considerable time after the storm has dissipated) was approximately 9%; that is, the reduced model describes the dominant portion of the solution of (2.2) as predicted by the expansion of section 4.

Figures 5 and 6 are plots of the geopotential ($m^2\ s^{-2}$) and eastward component of the wind ($m\ s^{-1}$) at the same three points as in Figs. 2 and 3 as a function of time. The dominant portion of the solution reaches a steady state after 12 h, so all the oscillations in the pressure and velocity after that time in the full system model are mainly due to gravity waves. Note that the amplitudes and periods of the pressure perturbations throughout the simulation are similar to those of the reduced system pressure perturbations. Figure 7 is a temporal evolution plot of the vertical velocity ($m\ s^{-1}$) at the same points as in Fig. 4, and Fig. 8 is the difference ($m\ s^{-1}$) between Figs. 7 and 4, so the amplitudes and periods of the gravity waves can be seen more clearly for the entire simulation. The magnitude of the deviations of the vertical velocity from the dominant portion of the solution ($0.03\ m\ s^{-1}$) is an order of magnitude smaller than the maximum magnitude of the vertical velocity in the dominant portion of the solution ($0.5\ m\ s^{-1}$). As mentioned in the introduction, although in this sense they are relatively small, the question remains as to their role in triggering other storms. Unfortunately, this will be difficult to ascertain because the vertical velocities associated with the gravity wave component of the solution are in the noise range of current wind profilers.

It should also be mentioned that only large-scale gravity waves were generated in the model as expected from the analysis in section 4. Figure 9 is a contour plot of the geopotential at the surface at 24 h. The contour interval is $2\ m^2\ s^{-2}$. The scale of the gravity waves is clearly much larger than the heating term in Fig. 1. Satellite observations show gravity waves following severe thunderstorms (Erickson and Whitney 1973), and the numerical solution for the simple heating given in (5.1) clearly produces a similar phenomenon.

The rigid top in the model is artificial but only serves to prevent gravity waves from escaping vertically. Thus there are even more gravity waves in the model than there would be in the atmosphere, yet the gravity waves still play a minor role in the solution and their periods are still the same as the heating. Additional simulations with the upper boundary doubled in height produced almost identical results for the first 12 h and did not change the conclusions.

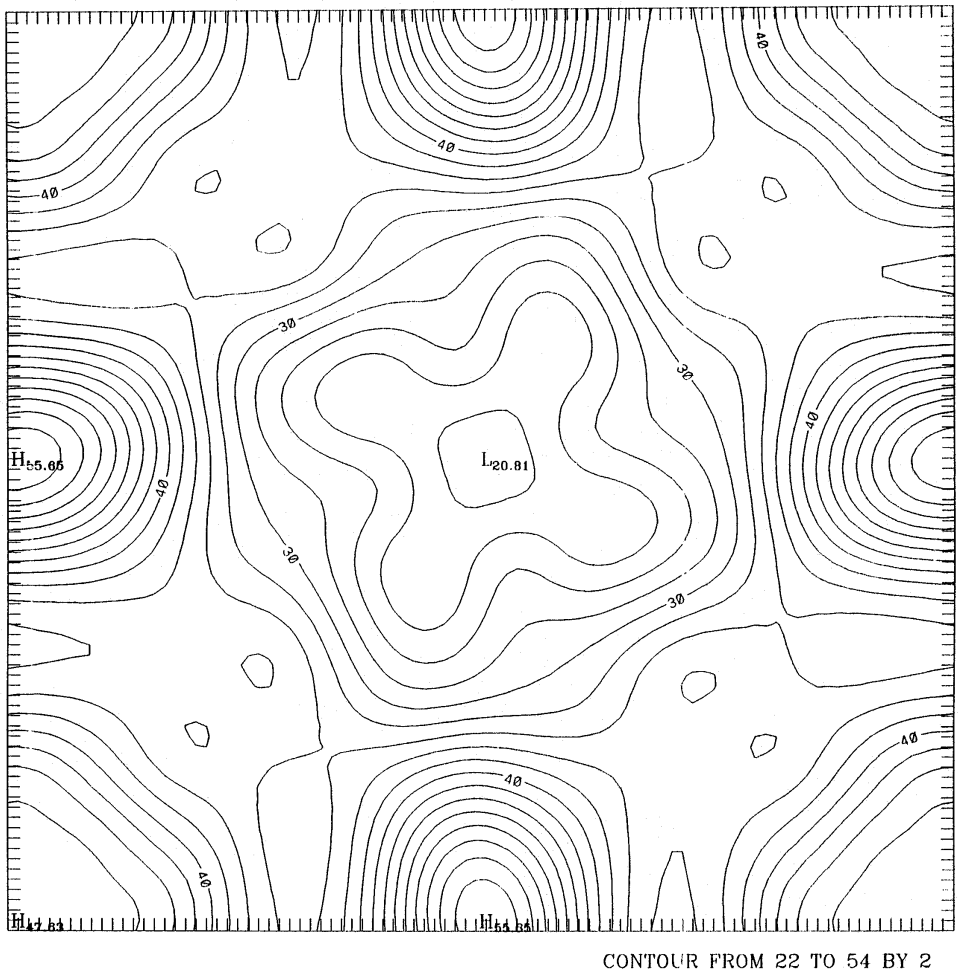

FIG. 9. The geopotential at the surface from the full system model at 24 h. The contour interval is 2 $m^2 s^{-2}$.

The previous section contains a proof that a model based on the multiscale system will accurately reproduce both the dominant and gravity wave portions of the solution of (2.2). The numerical approximation of the solution of (2.2) with the heating in (5.1) is considered to be the control for the following set of experiments; that is, it is the solution that would be obtained without any modification of the Eulerian equations. Centered second-order finite difference approximations of the dimensional forms of the multiscale systems (3.3) and (3.8) similar to (5.4) were used to develop numerical models based on those systems. The models were integrated in time and the errors relative to the control run were computed. At the time of maximal heating ($t = 6$ h), the relative l_2 errors in the velocity were approximately 3% and 1% for the model without and with a change of variable, respectively. Both errors are within the bounds predicted by the mathematical estimates. At the end of the run ($t = 24$ h), the errors were larger. The divergent component of the velocity was removed from the wind at the end of the control and multiscale model runs using the Helmholtz relations. The error then dropped to the 6-h level. The gravity wave plots for the models based on the multiscale systems are essentially identical to the gravity wave plot for the unmodified system. Figure 10 is a plot of the multiscale model geopotential ($m^2 s^{-2}$) at the same points as in Fig. 2 as a function of time. As can be clearly seen, Figs. 2 and 10 are very similar, even 12 h after the storm has dissipated. Although the gravity waves contain only a small part of the kinetic energy of the solution and to a very accurate approximation can be neglected in that part of the motion that has horizontal length scales similar to the heating, they are computed correctly by the multiscale system.

Figure 11 is a plot of the geopotential ($m^2 s^{-2}$) from the full system model in a domain 220 km in length and width ($I = J = 22$) at the three grid points with indices $A = (0, 0, 0)$, $B = (3, 3, 0)$, $C = (6, 6, 0)$ as a function of time. Point C of this plot is in the same location relative to the center of the storm as point C in Fig. 5. This plot shows that if a periodic domain smaller than the real case (here that is assumed to be the solution from the 900 km in length and width do-

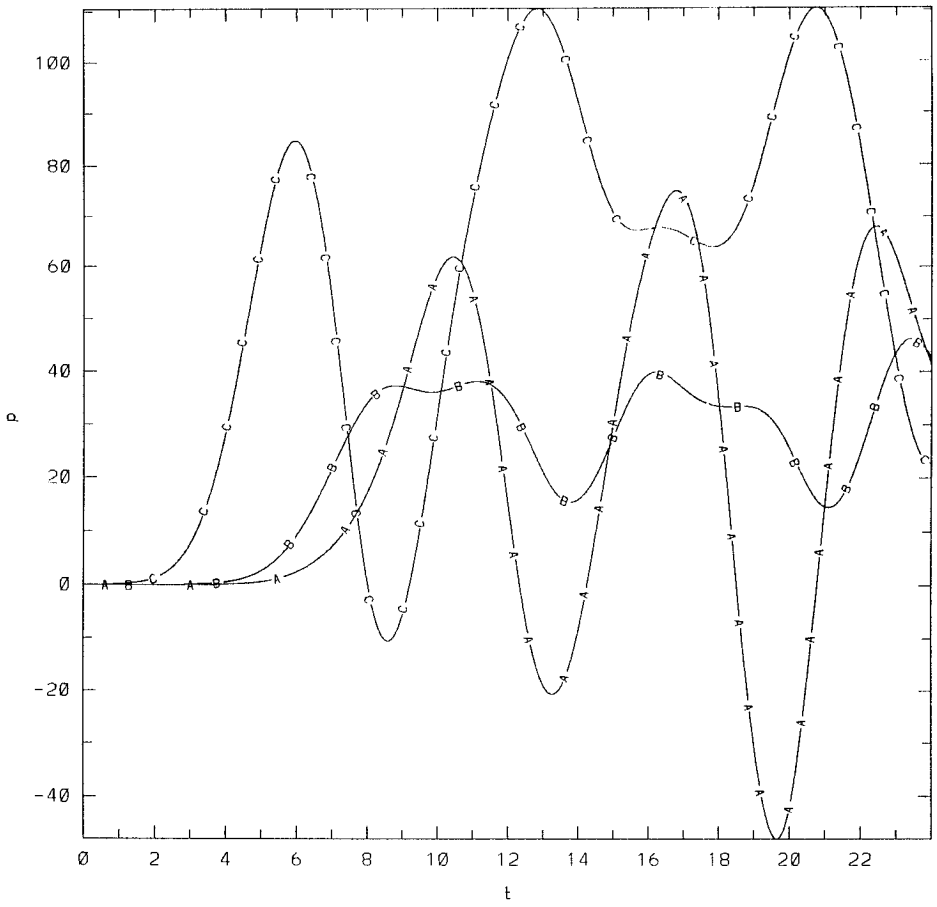

FIG. 10. The geopotential ($m^2\ s^{-2}$) from the multiscale system model plotted at the same grid points as in Fig. 2 as a function of time (h).

main) is used, a very different time evolution of the gravity waves will be computed. An open boundary model on a smaller domain must let the gravity waves propagate through the boundaries exactly as they would if the open boundary were not present, in order to compute the gravity waves correctly.

6. Conclusions

The two mesoscale cases where the lateral extent of the domain of solution is the same as or larger than the lateral extent of the mesoscale heating have been analyzed. In the first case, with appropriate initial and boundary conditions, only very small amplitude gravity waves are generated and it can be rigorously proved that they essentially do not interact with the reduced system component of the solution. In the second case, large-scale gravity waves with a timescale on the order of several hours (the same timescale as the reduced system component of the solution) are generated. The size of the pressure perturbation in the gravity wave component of the solution can be as large as the size of the pressure perturbation due to the reduced system component. Although many mesoscale phenomena have been classified as gravity waves based on temporal plots of the pressure at a single location, this result shows that it is very difficult to distinguish between the two components of the solution based on this criterion. Thus attempts to distinguish between the two components based solely on temporal information can lead (and has led) to considerable confusion. The mathematical analysis shows that the two components should not be distinguished by their variation in time, but rather by their variation in space. Also, the kinetic energy in the gravity wave component of the solution is much less than the kinetic energy in the reduced system component. However, if observing the wind at a location away from the location of the maximum wind velocities, the oscillations due to the gravity wave component can dominate and this also can lead to confusion. Note that these conclusions imply that different types of gravity waves will be obtained if different limited areas are used, and if these gravity waves are important, they must be generated correctly by using a domain sufficiently large to do so.

In either of the above cases, it has been proved that the solution is accurately described by the multiscale system for meteorology introduced by Browning and Kreiss (1986). In the case when the lateral extent of the

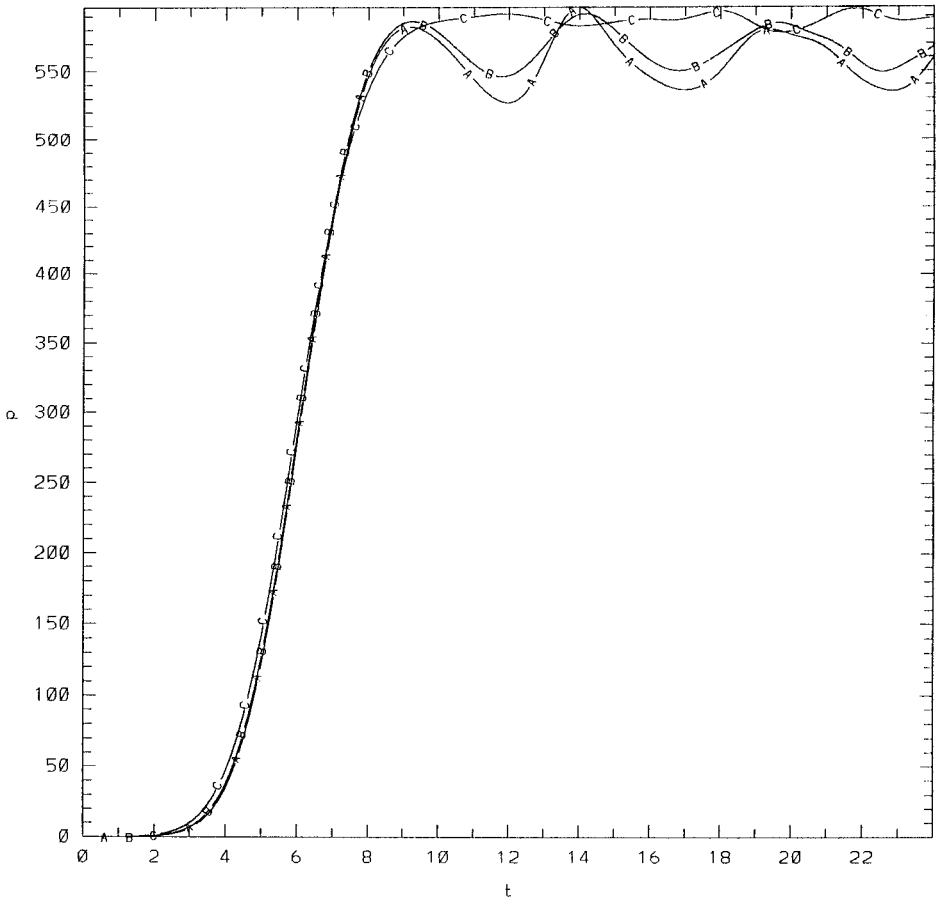

FIG. 11. The geopotential ($m^2\ s^{-2}$) from the full system model (in a smaller domain) plotted at the grid points $A = (0, 0, 0)$, $B = (3, 3, 0)$, and $C = (6, 6, 0)$ as a function of time (h). Point C is in the same location relative to the center of the storm as Point C in Fig. 5.

domain is larger than the lateral extent of the heating, the large-scale gravity waves that are generated are accurately computed by the multiscale model. If only interested in the dominant component of the solution, the reduced system can be used.

Acknowledgments. The work of G.L.B. was supported by the office of Naval Research under contract N00014-92-J-1089. The work of H.O.K. was supported by the National Science Foundation under Contract DMS 90-61311 and by the Office of Naval Research under Contract N00014-90-J-1382. The authors wish to express their appreciation to Roger Pielke for his excellent selection of competent reviewers and to those reviewers for their scientific objectivity.

REFERENCES

Bosart, L. F., and F. Sanders, 1986: Mesoscale structure in the megalopolitan snowstorm of 11–12 February 1983. Part III: A large amplitude gravity wave. *J. Atmos. Sci.,* **43,** 924–939.

Browning, G. L., and H.-O. Kreiss, 1985: Numerical problems connected with weather prediction. *Progress and Supercomputing in Computational Fluid Dynamics,* S. Abarbanel, R. Glowinski, G. Golub, P. Henrici, and H.-O. Kreiss, Eds., Birkhauser, 377–394.

——, and ——, 1986: Scaling and computation of smooth atmospheric motions. *Tellus,* **38A,** 295–313.

——, and A. E. MacDonald, 1993: Incorporating topography into the multiscale systems for the atmosphere and oceans. *Dyn. Atmos. Oceans,* **18,** 119–149.

——, and H.-O. Kreiss, 1994a: The impact of rough forcing on systems with multiple time scales. *J. Atmos. Sci.,* **51,** 369–383.

——, and ——, 1994b: Splitting methods for problems with different timescales. *Mon. Wea. Rev.,* **122,** 2614–2622.

——, and ——, 1996: An analysis of periodic updating for systems with multiple timescales. *J. Atmos. Sci.,* **53,** 335–348.

Brunk, I. W., 1949: The pressure pulsation of 11 April 1949. *J. Meteor.,* **6,** 181–187.

Clarke, R. H., 1962: Pressure oscillations and fallout down draughts. *Quart. J. Roy. Meteor. Soc.,* **88,** 459–469.

Daley, R., 1991: *Atmospheric Data Analysis.* Cambridge University Press, 457 pp.

Eom, J. K., 1975: Analysis of the internal gravity wave occurrence of April 19, 1970 in the Midwest. *Mon. Wea. Rev.,* **103,** 217–226.

Erickson, C. O., and L. F. Whitney, 1973: Gravity waves following severe thunderstorms. *Mon. Wea. Rev.,* **101,** 708–711.

Ford, R., 1994: Gravity wave radiation from vortex trains in rotating shallow water. *J. Fluid Mech.,* **281,** 81–118.

Gill, A. E., 1980: Some simple solutions for heat-induced tropical circulation. *Quart. J. Roy. Meteor. Soc.,* **106,** 447–462.

Houze, R. A., 1989: Observed structure of mesoscale convective systems and implications for large-scale heating. *Quart. J. Roy. Meteor. Soc.,* **115,** 425–461.

Kasahara, A., 1984: The linear response of a stratified global atmosphere to tropical thermal forcing. *J. Atmos. Sci.,* **41,** 2217–2237.

Kreiss, H.-O., and J. Lorenz, 1989: *Initial Boundary Value Problems and the Navier–Stokes Equations.* Academic Press, 402 pp.

——, ——, and M. J. Naughton, 1991: Convergence of the solutions of the compressible to the solutions of the incompressible Navier–Stokes equations. *Adv. Appl. Math.,* **12,** 187–214.

Ley, B. E., and W. R. Peltier, 1978: Wave generation and frontal collpase. *J. Atmos. Sci.,* **35,** 3–17.

Lindzen, R. S., and K. K. Tung, 1976: Banded convective activity and gravity waves. *Mon. Wea. Rev.,* **104,** 1602–1617.

Oliger, J., and A. Sundström, 1978: Theoretical and practical aspects of some initial-boundary value problems in fluid dynamics. *SIAM J. Appl. Math.,* **35,** 419–446.

Pothecary, I. J., 1954: Short period variations in surface pressure and wind. *Quart. J. Roy. Meteor. Soc.,* **80,** 181–187.

Ralph, F. M., M. Crochet, and S. V. Venkateswaran, 1993: Observations of a mesoscale ducted gravity wave. *J. Atmos. Sci.,* **50,** 3277–3291.

Sanders, F., and L. F. Bosart, 1985: Mesoscale structure in the megalopolitan snowstorm, 11–12 February 1983. Part II: Doppler radar study of the New England snowband. *J. Atmos. Sci.,* **42,** 1398–1407.

Skamarock, W. C., and J. B. Klemp, 1994: Efficiency and accuracy of the Klemp–Wilhelmson time-splitting technique. *Mon. Wea. Rev.,* **122,** 2623–2630.

Stobie, J. G., F. Einaudi, and L. W. Uccellini, 1983: A case study of gravity waves–convective storms interaction: 9 May 1979. *J. Atmos. Sci.,* **40,** 2804–2830.

Uccellini, L. W., and S. E. Koch, 1987: The synoptic setting and possible energy sources for mesoscale wave disturbances. *Mon. Wea. Rev.,* **115,** 721–729

Wagner, A. J., 1962: Gravity waves over New England. *Mon. Wea. Rev.,* **90,** 431–436.